

# Globalizing results from ocean in situ iron fertilization studies

Olivier Aumont, Laurent Bopp

▶ **To cite this version:**

Olivier Aumont, Laurent Bopp. Globalizing results from ocean in situ iron fertilization studies. Global Biogeochemical Cycles, 2006, 20 (2), pp.GB2017. 10.1029/2005GB002591 . hal-00138103

**HAL Id: hal-00138103**
**https://hal.science/hal-00138103**

Submitted on 17 Sep 2020

**HAL** is a multi-disciplinary open access archive for the deposit and dissemination of scientific research documents, whether they are published or not. The documents may come from teaching and research institutions in France or abroad, or from public or private research centers.

L'archive ouverte pluridisciplinaire **HAL**, est destinée au dépôt et à la diffusion de documents scientifiques de niveau recherche, publiés ou non, émanant des établissements d'enseignement et de recherche français ou étrangers, des laboratoires publics ou privés.

# Globalizing results from ocean in situ iron fertilization studies

O. Aumont[1] and L. Bopp[2]

Received 22 July 2005; revised 19 January 2006; accepted 10 February 2006; published 14 June 2006.

[1] Despite the growing number of in situ iron fertilization experiments, the efficiency of such fertilization to sequester atmospheric $CO_2$ remains largely unknown. For the first time, a global ocean biogeochemical model has been evaluated against those experiments and then used to estimate the effect of a long-term and large-scale iron addition on atmospheric $CO_2$. The model reproduces the observed timing and amplitude in chlorophyll, the shift in ecosystem composition, and the $pCO_2$ drawdown; it also proves to be of utility in interpreting the observations. However, a full ocean fertilization during 100 years results in a 33 μatm decrease in atmospheric $CO_2$, that is 2 to 3 times smaller than found previously.

**Citation:** Aumont, O., and L. Bopp (2006), Globalizing results from ocean in situ iron fertilization studies, *Global Biogeochem. Cycles*, *20*, GB2017, doi:10.1029/2005GB002591.

## 1. Introduction

[2] For about 2 decades now, iron has been increasingly highlighted as a major element in the ocean biogeochemistry regulating the ocean productivity over large areas of the oceans [e.g., *Martin and Fitzwater*, 1988; *Martin et al.*, 1990; *Coale et al.*, 1996]. The most striking demonstration that iron limits oceanic phytoplankton growth has been given by the mesoscale iron fertilization experiments that were conducted in the three major HNLC (high nutrient–low chlorophyll) regions: the Southern Ocean [*Boyd et al.*, 2000; *Gervais et al.*, 2002; *Coale et al.*, 2004], the eastern equatorial Pacific [*Martin et al.*, 1994; *Coale et al.*, 1996] and the subarctic Pacific [*Tsuda et al.*, 2003; *Boyd et al.*, 2004]. Despite large differences in the magnitude of the response, virtually all experiments have provoked a large increase in chlorophyll, generally dominated by diatoms, and a strong decrease in surface $pCO_2$ [*de Baar et al.*, 2005].

[3] Even if all iron fertilization experiments have led to a significant increase in the phytoplankton biomass, the fate of this fixed carbon remains quite unclear. During SOIREE, no detectable increase in export production was observed [*Nodder et al.*, 2001] whereas at IRONEXII, a more than a seven-fold increase was diagnosed [*Bidigare et al.*, 1999]. The magnitude of the export increase is not the only important parameter to infer the additionally sequestered carbon. Of critical importance also is the depth at which the organic carbon is exported which will determine the timescale for which carbon is trapped in the ocean. Unfortunately, no usable information is yet available on that aspect.

[4] Despite these uncertainties, the success of the in situ iron fertilization experiments has given support to the idea of artificially fertilizing the ocean to mitigate the atmospheric $CO_2$ increase resulting from the anthropogenic activities [*Gribbin*, 1988; *Martin*, 1990]. Since then, this idea has caused a considerable debate, mostly because the sparse and short-term iron fertilization experiments are difficult to interpret in terms of the massive iron addition that would be necessary to affect atmospheric $CO_2$ [e.g., *Chisholm et al.*, 2001; *Buesseler and Boyd*, 2003]. Another argument in this debate is that iron fertilization may have potential side effects that could partly or totally cancel out its potential benefits, as, for instance, increased anoxia or hypoxia of the intermediate and deep ocean [e.g., *Sarmiento and Orr*, 1991; *Jin and Gruber*, 2003; *Gnanadesikan et al.*, 2003].

[5] Simplistic global biogeochemical models have been used to evaluate the effect of long-term, large-scale iron fertilization. However, these models attempted only to estimate a maximum effect, that is, they assumed that surface macronutrients in HLNC regions were depleted to zero all year round [*Peng and Broecker*, 1991; *Joos et al.*, 1991; *Sarmiento and Orr*, 1991; *Matear and Wong*, 1999] or 6 months a year [*Kurz and Maier-Reimer*, 1993]. They suggest that such massive fertilization could reduce atmospheric $CO_2$ by at least 50 ppmv and by up to 107 ppmv after 100 years of fertilization (Table 1). Thus, even in these extreme unlikely scenarios, fertilization does not appear to provide the cure to our carbon imbalance problem. Nevertheless, the simulated reduction in atmospheric $CO_2$ is far from being negligible and may still seem attractive as one among the different available means to trap anthropogenic carbon.

[6] A demonstration of such an intact attraction is given by the numerous existing proposals to commercially exploit purposeful iron infusions (see *Chisholm et al.* [2001] for a list of some of them). However, the model estimates are most likely to be an upper limit. Recently, *Zeebe and Archer* [2005] have proposed a more realistic estimate of the

[1]Laboratoire d'Océanographie et de Climatologie: Expérimentation et Approches Numériques, IRD/IPSL, Plouzané, France.
[2]Laboratoire des Sciences du Climat et de l'Environnement, CNRS/IPSL, Gif-sur-Yvette, France.

Copyright 2006 by the American Geophysical Union.
0886-6236/06/2005GB002591

**Table 1.** Atmospheric Reduction in $CO_2$ Due to Iron Fertilization Estimated by Seven Models Forced With an IPCC Business-as-Usual Emissions Scenario

| | Model Type[a] | Atmospheric $CO_2$, ppmv | Ocean Uptake, GtC |
|---|---|---|---|
| *Sarmiento and Orr* [1991] | 3-D | 72 | 153 |
| *Kurz and Maier-Reimer* [1993] | 3-D | 50 | 106 |
| *Matear and Wong* [1999] | 3-D | 75 | 159 |
| *Joos et al.* [1991] | BM | 107 | 227 |
| *Peng and Broecker* [1991] | BM | 64–96 | 136–204 |

[a]Abbreviations: 3-D, 3-D ocean model; BM, box model.

efficiency of iron fertilization. Using the results from SOFEX [*Coale et al.*, 2004] and simple ocean biogeochemical models, they have evaluated to 15 ppmv the maximum reduction in atmospheric $CO_2$ that can be realistically expected from iron fertilization. This drawdown is much lower than what was simulated by the previous modeling studies. However, their work is based on very simplified ocean carbon-cycle models and on only one in situ experiment which may not be representative of the whole Southern Ocean and of longer-term iron enrichment.

[7] In the last few years, several global ecosystems models have been developed that include an explicit representation of the iron cycle [e.g., *Moore et al.*, 2002; *Aumont et al.*, 2003; *Gregg et al.*, 2003; *Dutkiewicz et al.*, 2005]. Despite their simplicity, especially in their description of the iron chemistry, they have proved to be able to reproduce the main characteristics of the HNLC regions as well as the major patterns of the global iron distribution. These models offer now the potential to explicitly assess the effects of iron fertilization. In this study, we will initially focus on the in situ iron enrichment experiments by simulating the time evolution of short-term patchy iron additions. The objectives are (1) to evaluate the model and (2) to also use the model to help analyze the results from the eight iron fertilization experiments for which results have been published so far. In a second step, iron fertilization has been performed over the global ocean for a hundred years to forecast its efficiency to mitigate atmospheric $CO_2$ increase.

## 2. Model Description

### 2.1. Physical Model

[8] We use the ocean model ORCA2-LIM, which is based on the ORCA2 global configuration of OPA version 8.2 [*Madec et al.*, 1998] coupled to the dynamic-thermodynamic ice model developed at Louvain-La Neuve [*Timmermann et al.*, 2003]. The ocean model has a mean horizontal resolution of about 2° by 2° cos$\phi$ (where $\phi$ is the latitude) with a meridional resolution enhanced to 0.5° at the equator. The model has 30 vertical levels, increasing from 10 m at the surface to 500 m at depth. Twelve levels are located in the top 125 m. The effects of unresolved mesoscale eddies are parameterized following the parameterization of *Gent and McWilliams* [1990] poleward of 10° latitude. Lateral mixing both on tracers and momentum is performed along isopycnal surfaces as in the work by *Lengaigne et al.* [2003]. The flow of deep water over bathymetry is represented using the bottom boundary layer (BBL) proposed by *Beckmann and Döscher* [1997]. Vertical eddy and viscosity coefficients are computed from the prognostic model of turbulent kinetic energy (TKE) of *Blanke and Delecluse* [1993].

[9] Climatological atmospheric forcing are constructed from various data sets consisting of daily NCEP/NCAR 2m atmospheric temperature averaged over 1948–2003 [*Kalnay et al.*, 1996], monthly relative humidity [*Trenberth et al.*, 1989], monthly ISCCP total cloudiness averaged over 1983–2001 [*Rossow and Schiffer*, 1999], monthly precipitation averaged over 1979–2001 [*Xin and Arkin*, 1997], and weekly wind stress based on ERS satellite product and TAO observations [*Menkes et al.*, 1998]. Surface heat fluxes and evaporation are computing using empirical bulk formulas described by *Goose* [1997]. To avoid any strong model drift, modeled sea surface salinity is restored to the monthly WOA01 data set [*Conkright et al.*, 2002] with a timescale of 40 days. The ocean model has been spun up for 200 years.

### 2.2. Ocean Biogeochemical Model

[10] In this study, we use the Pelagic Interaction Scheme for Carbon and Ecosystem Studies (PISCES) ocean biogeochemical model. This model is derived from the Hamburg Model of Carbon Cycle version 5 (HAMOCC5) [*Aumont et al.*, 2003]. As a detailed description of the model parameterizations is provided as auxiliary material[1], the model will be only briefly presented here. PISCES is constructed on the assumption that phytoplankton growth is directly limited by the external availability in nutrients [*Monod*, 1942]. This choice was mostly dictated by the computing cost as PISCES has been designed to suit a wide range of temporal and spatial scales, including quasi steady state simulations on the global scale.

[11] The model has 24 compartments (Figure 1). Phytoplankton growth can be limited by five different nutrients: nitrate, ammonium, phosphate, silicate and iron. Four living pools are represented: two phytoplankton size classes/groups (nanophytoplankton and diatoms) and two zooplankton size classes (microzooplankton and mesozooplankton). Diatoms differ from nanophytoplankton by their need in Si, by higher requirements in Fe [*Sunda and Huntsman*, 1995] and by higher half-saturation constants because of their larger mean size. For all living compartments, the ratios between C, N and P are kept constant to the values proposed by *Takahashi et al.* [1985]. On the other hand, the internal contents in Fe of both phytoplankton groups and in Si of diatoms are prognostically simulated as a function of the external concentrations in nutrients and of

[1]Auxiliary material is available at ftp://ftp.agu.org/apend/gb/2005gb002591.

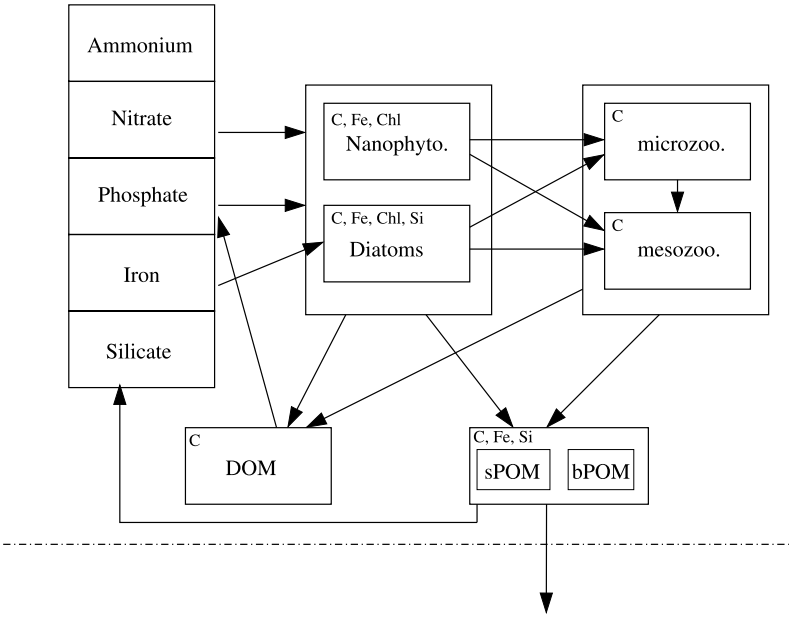



**Figure 1.** Schematic description of the PISCES ecosystem model. Not all the flows between the different compartments are drawn. The elements listed in the upper left corner of the boxes represent the explicitly modeled currencies in each pool.

the light level. The $\frac{Chl}{C}$ ratio is modeled using a modified version of the photoadaptation model by *Geider et al.* [1998]. All the elemental ratios of zooplankton are kept constant.

[12] There are three nonliving compartments: semilabile dissolved organic matter (with timescales of several weeks to several years), small and big sinking particles. The two particle size classes differ by their sinking speeds (3 m/d for the small size class and 50 to 200 m/d for the large size class). As for the living compartments, constant Redfield ratios are imposed for C/N/P. However, the iron, silicon and calcite pools of the particles are fully simulated. As a consequence, their ratios relative to organic carbon are allowed to vary. The impact of ballast minerals on particles sinking speeds is not accounted for in the model [e.g., *Armstrong et al.*, 2002].

[13] Nutrients are supplied to the ocean from three different sources: atmospheric dust deposition, rivers and sediment mobilization. These sources are explicitly modeled and are extensively described in the supplementary material. Thus only the main aspects are presented here. Iron deposition from the atmosphere has been estimated from the climatological monthly maps of dust deposition simulated by the model of *Tegen and Fung* [1995] assuming constant values for the iron content and the solubility [e.g., *Jickells and Spokes*, 2001; *Moore et al.*, 2004]. River discharge of carbon is taken from the Global Erosion Model (GEM) of *Ludwig et al.* [1996]. Fe, N, P and Si supplies are derived from the same model output by considering globally constant Fe/P/N/Si/C ratios in the rivers. Reductive mobilization of iron from marine sediments have been recognized as a significant source to the ocean [e.g., *Johnson et al.*, 1999; *de Baar and de Jong*, 2001]. Unfortunately, almost no quantitative information is available to describe this potentially important source. In a way similar to *Moore et al.* [2004], we have very crudely parameterized this input of iron.

### 2.3. Iron Fertilization Experiments

[14] Phosphate, oxygen, nitrate and silicic acid distributions have been initialized at uniform concentrations inferred from observed climatologies [*Conkright et al.*, 2002]. Initial values for dissolved inorganic carbon and alkalinity are taken from the OCMIP guidelines [*Orr*, 1999]. The ecological tracers are initialized uniformly to arbitrary low values. Iron concentrations are set everywhere to 0.6 nM. The model is then spun up offline for 3000 years using the dynamics predicted by the dynamical model. After this integration, primary productivity as well as $CO_2$ fluxes drift by less than 0.01 GtC $yr^{-1}$.

[15] In a first set of experiments, patchy iron fertilization experiments have been performed. The fertilizing sites have been selected in the three main HNLC regions defined as follows: south of 40°S for the Southern Ocean, between 180°W and 80°W and between 5°S and 5°N for the equatorial Pacific, and north of 40°N and between 140°E and 120°W for the subarctic North Pacific. In each of these three regions, iron has been added in one grid cell of the model every 10° in longitude and 5° in latitude. The spatial distribution of all the infusion sites can be seen in Figure 6 in section 4.1. At each site, iron concentration is set to 2 nM in the whole mixed layer on day 2.5 and maintained to that value for the rest of the simulation which has a total duration of 45 days. These patchy iron fertilization experiments have been repeated every month starting from unperturbed initial states.

[16] In a second step, a massive large-scale and long-term iron fertilization has been simulated. In this experiment, iron

is set to 2 nM in the mixed layer everywhere and maintained to that value for 100 years starting in 2000. The ocean model exchanges $CO_2$ with an interactive atmospheric box forced by fossil fuel emissions from IPCC scenario SRES98-A2 [*Nakisenovic et al.*, 2000] and continental biospheric carbon fluxes derived from a fully coupled carbon-climate run using the same IPCC scenario [*Dufresne et al.*, 2002]. The initial state of this experiment has been obtained from a 100-year simulation, beginning thus in 1900. In this prefertilization run, we have used observed fossil fuel emissions and biospheric fluxes from the same fully coupled carbon-climate run than in the massive iron fertilization experiment. In both the pre- and post-2000 experiments, $CO_2$ concentration in the interactive atmospheric box is updated at the end of each year using the fossil-fuel emissions, the biospheric carbon fluxes and the air-sea $CO_2$ fluxes from our ocean model.

[17] Two additional sensitivity experiments have been performed for comparison with the massive fertilization experiment. In the first test, the ocean is never artificially iron fertilized. This experiment was designed to evaluate the impact of the massive iron fertilization on atmospheric $pCO_2$. In a second test, the ocean is supplied with iron for 10 years from 2000 to the end of 2009. Fertilization is then stopped for the rest of the 100 years run. This simulation was performed to estimate the timescale of the carbon sequestration. Except for these changes in the artificial iron supply, the experimental design of these tests is identical to our standard case.

## 3. Model Mean State

[18] The objective of this section is not to present an exhaustive validation of the model results. We rather illustrate some aspects of the model behavior that are of relevance in the framework of this study. The reader interested in a more complete description of the model output could refer to the auxiliary material or to the PISCES website (http://www.lodyc.jussieu.fr/∼aumont).

### 3.1. Iron

[19] Figure 2 shows the distribution of iron at the surface and at 1000 m depth for the model ocean and for the scarce available observations. In the open ocean, the highest surface iron concentrations are simulated in the North Atlantic and in the North Indian basins in agreement with the observations. These elevated values are created by the strong local aeolian source, especially from the Sahara desert. However, the maximum modeled iron levels are in general underestimated relative to the observations. Surface values higher than 0.8 nM have been measured both in the Atlantic Ocean [*Vink and Measures*, 2001; *Sarthou et al.*, 2003] and in the Indian Ocean [*Measures and Vink*, 1999] whereas in the model, they hardly exceed 0.5 nM. Over the rest of the open ocean, iron concentrations are low, generally below 0.2 nM as a result of low aeolian input and/or upwelling of iron depleted waters. Elevated Fe levels are produced on the continental margins by the imposed sediment source, in broad agreement with the very sparse available data [e.g., *Sedwick et al.*, 2000; *Nishioka et al.*, 2001].

[20] Deeper in the water column, at 1000 m, the modeled iron distribution is in qualitative agreement with the quite sparse observations (Figure 2b). Iron concentrations are relatively high in the North Atlantic and in the North Pacific with values ranging between 0.7 and 1 nM. Modeled iron values are generally higher in the Atlantic relative to the Pacific and seem to be slightly overestimated compared to the data. The modeled iron distribution exhibits decreasing concentrations to the south. Minimum middepth concentrations are simulated in the Southern Ocean in agreement with the data, despite the fact that they appear to be overpredicted by the model. Our modeled distribution at 1000 m resembles quite strongly that of *Parekh et al.* [2004]. This is not surprising as both parameterizations of the iron cycle in the water column are based on the same assumptions and are thus similar.

### 3.2. Chlorophyll

[21] Modeled chlorophyll distribution is compared to the SeaWiFS satellite observations for May and November (Figure 3). The observed patterns are qualitatively reproduced by the model. Slightly too low chlorophyll concentrations are predicted in the subtropical oligotrophic gyres. In two of the three major HNLC regions, i.e., the equatorial Pacific and the Southern Ocean, the model succeeds in reproducing the quite moderate chlorophyll levels associated with elevated macronutrients. In the Southern Ocean, the simulated chlorophyll standing stock seems to be too elevated during the growing season. A possible explanation may be the overpredicted middepth iron concentrations which lead to an excessive accumulation during winter. In the subarctic Pacific Ocean, the third major HNLC region, chlorophyll surface concentrations are largely underestimated all year round, especially in the eastern part of the basin. As in most coarse-resolution models [*Aumont et al.*, 2002; *Gnanadesikan et al.*, 2002; *Dutkiewicz et al.*, 2005], the ocean dynamics in this region is not correctly reproduced. The Kuroshio current separates from the coast much too far to the north, bringing to the subarctic Pacific too warm, too salty and nutrient-poor subtropical waters [*Gnanadesikan et al.*, 2004].

[22] During boreal spring, chlorophyll concentrations are high in the mid and high latitudes of the North Atlantic Ocean. Maximum levels appear to be overestimated, especially in the most northern part of the basin. Chlorophyll concentrations are generally strongly underestimated in the eastern coastal upwelling region as the model resolution is too coarse to correctly resolve the dynamics of these regions. Nevertheless, this underestimation becomes even worse when no iron supply from the sediments is included confirming the critical importance of this source to sustain the observed high levels of phytoplankton standing stock in the coastal upwellings [e.g., *Hutchins and Bruland*, 1998; *Bruland et al.*, 2005].

## 4. Iron Fertilization Experiments

### 4.1. Patchy Iron Fertilization

[23] The model response to these patchy Fe additions is illustrated on Figure 4 for two groups of sites similar in their

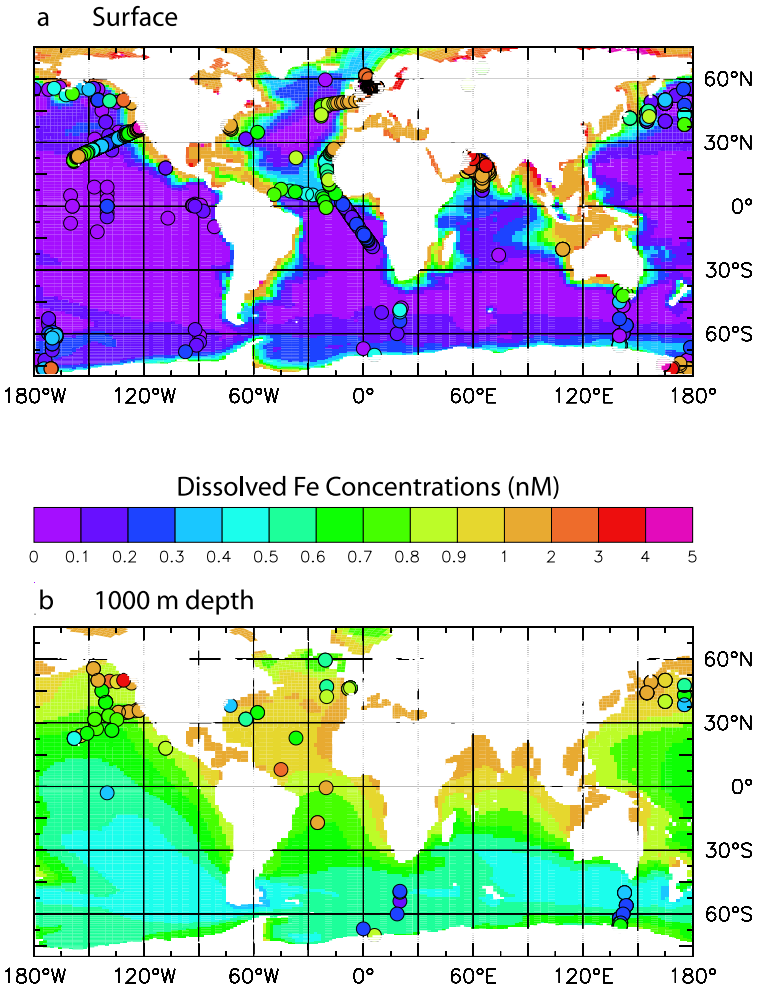



**Figure 2.** Comparison to observations: dissolved iron (in nM) from PISCES, annual mean (a) at the surface and (b) at 1000 m depth. Available observations, mainly based on work by *Parekh et al.* [2004] compilation are displayed as dots with the same color code.

biogeochemical and physical conditions to IRONEXII [*Coale et al.*, 1996] in the equatorial Pacific (Figure 4a) and SOIREE [*Boyd et al.*, 2000] in the Southern Ocean (Figure 4b). These sites have been selected because they strongly differ in their physical and biogeochemical conditions. As a consequence, the responses to the iron addition are quite different. The model simulates a large and rapid increase in chlorophyll after the fertilization similar in magnitude to the observations. Both in the model and in the observations, the maximum chlorophyll is reached after 5–6 days at IRONEXII, and after 13–14 days at SOIREE. Most of the biomass increase is due to diatoms which account for more than 60% of the maximum total biomass as observed [e.g., *Cavender-Bares et al.*, 1999; *Gall et al.*, 2001]. As a result of these blooms, surface $pCO_2$ substantially decreases at both sites, in good agreement with the data. An encouraging result from this simple illustration is the success of the model in producing quite contrasted responses to iron fertilization as observed.

[24] Even if all the in situ experiments resulted in a significant increase in chlorophyll, the magnitude of this response strongly differs between sites: from 2.5 mg Chl/$m^3$ at SOIREE [*Boyd et al.*, 2000] to more than 19 mg Chl/$m^3$ at SEEDS [*Tsuda et al.*, 2003]. These differences are largely explained by differences in the mixed layer [*Platt et al.*, 2003; *de Baar et al.*, 2005]. That is, blooms following iron injection are stronger when the mixed layer depth is shallower (Figure 5a). Such a relationship supports the hypothesis that the light limitation arising from the auto-shading by the phytoplankton triggers the end of the bloom onset. However, insufficient data are available to confirm that hypothesis. When adding the model results to the experimental data, a similar relationship between mixed layer depth and chlorophyll is found. For a given mixed layer depth, the model exhibits substantial scatter below an apparent upper limit. This limit is well approximated by numerically solving the simple model of *Platt et al.* [2003], which relates the maximum phytoplankton

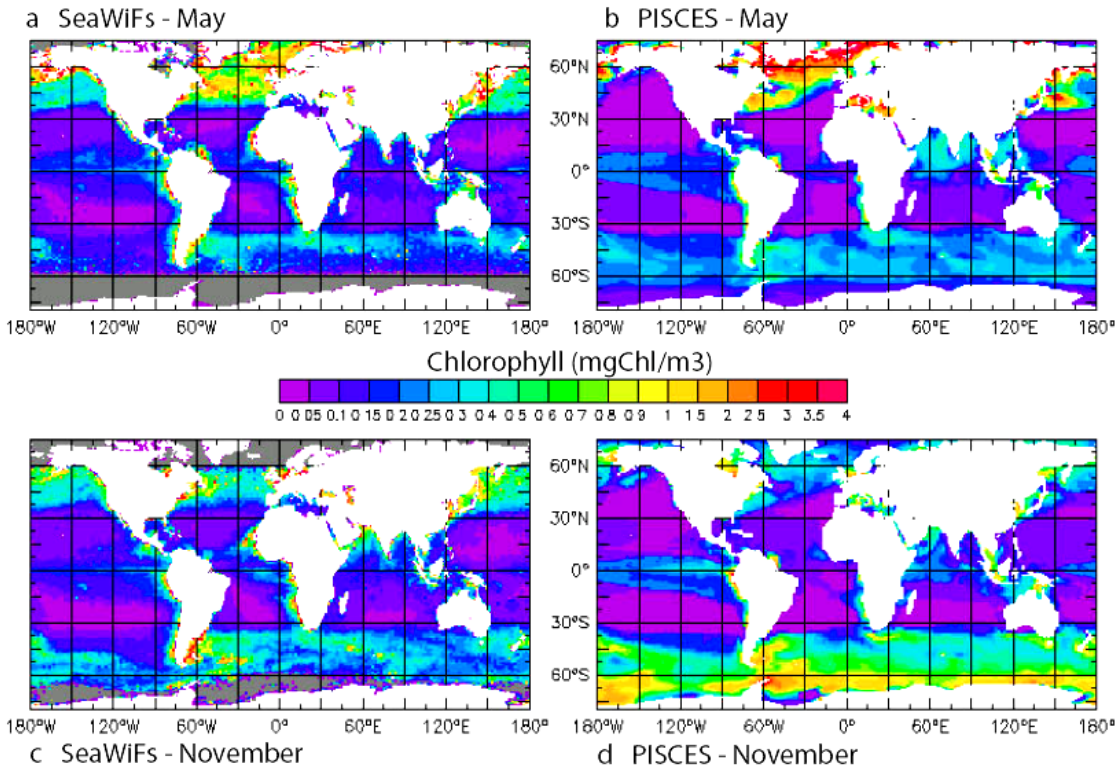



**Figure 3.** Comparison to observations: surface chlorophyll (in mg $m^{-3}$) derived from remote sensing (SeaWiFS) over 1997–2003 for (a) May and (c) November, compared to simulated chlorophyll from PISCES for (b) May and (d) November.

biomass to the light availability, and thus to the mixed layer depth (Figure 5a). However, mixed layer depth is not the only control of bloom intensity as other limiting factors often reduce this expected maximum response. For instance closer inspection of the model results reveals that limitation by silicate stops the bloom below this maximum value on the northern edge of the Southern Ocean and in the equatorial Pacific. This result is consistent with the findings of studies suggesting seasonal or intermittent silicon limitation of phytoplankton growth in these regions [*Dugdale and Wilkerson*, 1998; *Franck et al.*, 2000].

[25] One of the most important results of iron fertilization was the demonstration that fertilization has always led to a large decrease in sea surface $pCO_2$, from roughly 25 μatm in the Southern Ocean [*Bozec et al.*, 2005] to more than 90 μatm at SEEDS [*Tsuda et al.*, 2003]. Both the model results and the data show a clear relationship between bloom intensity and $CO_2$ drawdown (Figure 5b). In addition, our model shows that most of simulated carbon uptake is not exported but accumulated in the living biomass, and to a lesser extent in the dissolved organic pool. The export of organic matter to the subsurface contributes on average to only 25% of the DIC drawdown, which supports budget computations from in situ observations [*Tsuda et al.*, 2003; *Boyd et al.*, 2004; *Buesseler et al.*, 2004]. Although small during the whole course of the experiment, the contribution of the export tends to increase with time from an average of about 15% (15 days after the beginning of the fertilization) to the maximum mean value of 25% (reached on average after about 30 days).

[26] The duration of the bloom development is another feature of the iron fertilization experiments that displays considerable variability [*Boyd*, 2004]. At IRONEXII, maximum bloom intensity was reached after 5–6 days, whereas such took more than 2 weeks in the Southern Ocean (Figure 5c). Temperature should clearly play a critical role as, on average, phytoplankton growth rate increases with temperature. However, SEEDS demonstrated that the ecosystem composition is also critical since, during this experiment, diatoms were growing much more quickly than expected [*Tsuda et al.*, 2003]. Furthermore, despite a general trend to more rapid responses with increasing temperatures, the model simulates considerable variations between sites with the same SST (Figure 5c). However, the same temperature-growth rate formulation is prescribed for the two modeled phytoplankton groups. In fact, many factors control the net phytoplankton growth rate and its temporal evolution such as the grazing pressure, the available light, the initial nutrient concentrations. Consequently, the duration of the onset, optimum and decline of the bloom should show considerable variability between sites and should prove to be extremely difficult to predict a priori.

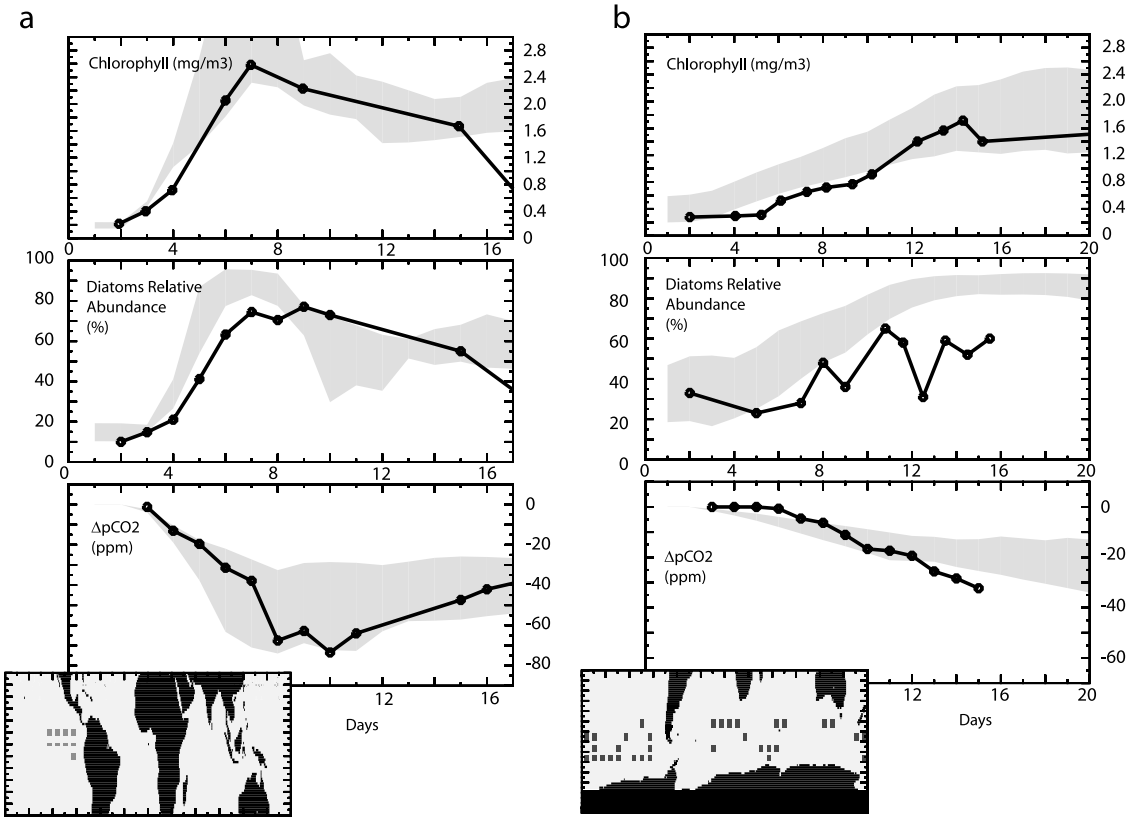



**Figure 4.** Evolution of some biogeochemical signals (mean chlorophyll, diatoms contribution, and surface $pCO_2$) at (left) IRONEXII and (right) SOIREE. The dots on all panels denote the observations. The gray shaded area indicates the range in the model responses: For each of the two fertilization experiments, all the injection sites in the model that have similar mixed layer depth (±10 m) and SST (±2°C), have been selected (nine sites for IRONEXII and 33 sites for SOIREE). Their locations are shown on the maps at the bottom of each column of figures. Iron has been added in the model at the same month than in the data (February for SOIREE and May for IRONEXII). Both the model output and the observations are displayed so that the first iron infusion occurs on day 2.5. Chlorophyll (top panels) is expressed as mean mixed-layer concentrations. Diatom contribution (middle panels) is shown as a percentage of the total Chl *a*. Difference in $pCO_2$ (bottom panels) is defined for the model as the difference between the fertilization experiment and a control experiment.

[27] Although all in situ experiments have shown that iron addition in HNLC regions stimulates the carbon fixation by phytoplankton, the fate of fixed carbon remains unclear. At SOIREE, there was no detectable increase in export production [*Boyd et al.*, 2000], whereas at IRONEXII there was more than a sevenfold increase [*Bidigare et al.*, 1999]. Our model also simulates large differences between the fertilization sites (Figure 5d). Both changes in the standing stock and in the mean sinking speed of the particles explain this important variability. For instance, the mean sinking velocities (which depends in our model on the relative contribution of the two modeled size classes of POC) increases at SOIREE-like sites by 4 to 11 m/day, i.e., by 30% up to 200%. These large differences result from numerous factors related to ecosystem structure and its physiological status. Most important factors are the initial biomasses of phytoplankton and zooplankton, the initial nutrients concentrations, the growing conditions like the temperature and the depth of the mixed layer. The respective role and the interplay of these factors are quite complex and vary a lot between the sites. Such complexity explains the large variability in the simulated response of export production.

[28] Nevertheless, an important rise in POC export is always predicted over the 45 days of the continuous iron addition with, on average, larger export as the bloom is stronger. Differences among in situ studies may be partly explained by their different sampling periods. Some studies have been probably too short in time to detect any change in export [*Buesseler et al.*, 2004]. The model supports this explanation as after 15 days, the increase in export is generally small, below 50%, and is not correlated with the maximum magnitude of the bloom or of the export production (Figure 5d). Thus there is a delay both between the maxima of biomass and export and between the onset of the

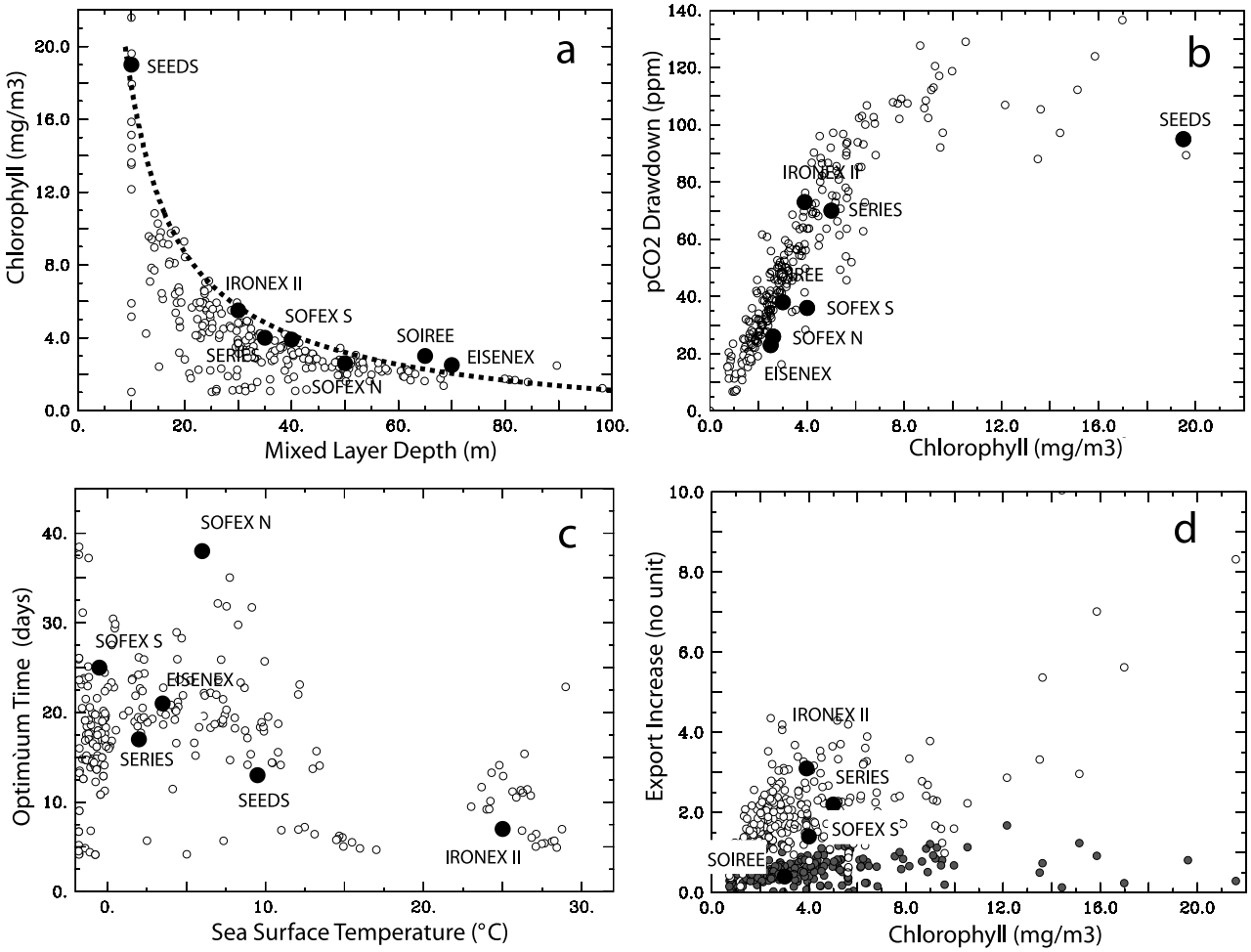



**Figure 5.** Maximum responses to iron injection in the observations (black dots) and in the model (open dots). We have selected seven fertilization experiments: IRONEX2 [*Coale et al.*, 1996], SOIREE [*Boyd et al.*, 2000], EISENEX [*Gervais et al.*, 2002], SEEDS [*Tsuda et al.*, 2003], two sites for SOFEX [*Coale et al.*, 2004], and SERIES [*Boyd et al.*, 2004]. IRONEXI [*Martin et al.*, 1994] has been excluded from the comparison because of water mass subduction that prevents the triggered bloom to develop. (a) Maximum surface chlorophyll as a function of the mean mixed layer depth. The dashed curve shows the relationship according to *Platt et al.* [2003] (see text). (b) Maximum surface drawdown in surface $pCO_2$ as a function of the maximum surface chlorophyll concentration. (c) Duration of the bloom development defined as the number of days necessary to reach the maximum chlorophyll concentration since the first iron addition as a function of sea surface temperature. (d) Maximum increase in export production as a function of the maximum surface chlorophyll concentration. This increase is defined as the ratio of the difference in export productions after and before the fertilization over the prefertilization export production. The gray dots show this increase in the model 13 days after the iron infusion.

bloom and the increase in export production. These gaps are highly variable between sites but are generally comprised between 10 and 20 days in the model. Estimations of the impact of iron fertilization on export of organic matter requires a sampling duration that extends well beyond the response of the phytoplankton community (at least another 20 days).

[29] All the in situ experiments have been performed during the favorable season in the Southern Ocean. They have all led to a significant biomass increase. However, one expects that in that region, the response of the biological activity to the iron stimulation should be highly seasonal. This hypothesis is supported by the relationship between the mixed layer depth and the maximum chlorophyll concentration which highlights the critical role of light limitation. As expected, the stimulation is restricted in the Southern Ocean to the summer season. This favorable period increases to the north from about 3 months off the Antarctic Coast to about 6 months north of the Polar Front (Figure 6). In the equatorial Pacific, the seasonality is much weaker: Phytoplankton blooms are generated by iron enrichment all year round. In the North Pacific, phytoplankton almost

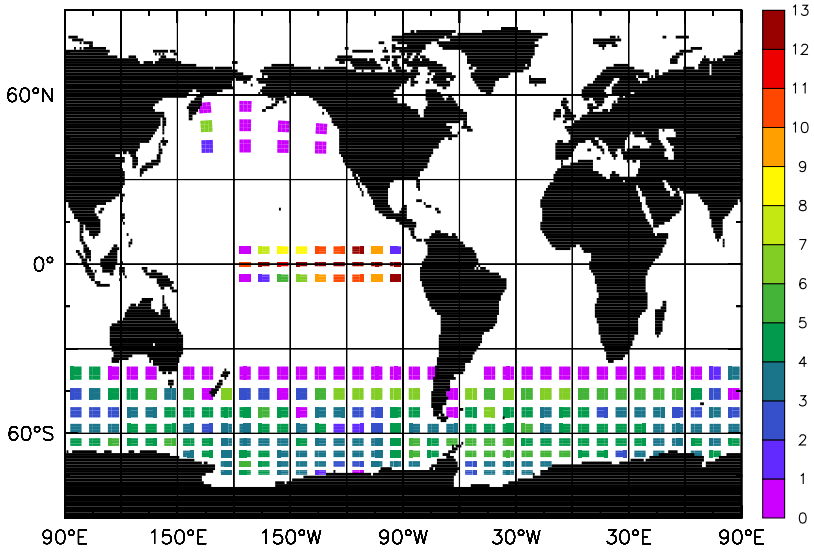



**Figure 6.** Number of months for which a strong biomass increase is simulated after iron addition (chlorophyll increase exceeds 1 mg Chl/$m^3$).

never responds to iron stimulation as a consequence of deficiencies in the simulated dynamics (see section 3).

### 4.2. Global Iron Fertilization

[30] In the first part of this study, we have shown that the model reproduces qualitatively and quantitatively the main features of the mesoscale experiments. It also proved to be of utility in interpreting the observations. In a second step, we have used the same model to assess the maximum long-term impact of massive iron fertilization on atmospheric $CO_2$. Thus we have designed another experiment in which the ocean model is supplied with iron everywhere in the mixed layer and for 100 years starting in year 2000. Results are then compared to another simulation using the same experimental design but without iron fertilization.

[31] As expected from the patchy fertilization experiments, the global primary productivity increases sharply from 41 GtC/yr to more than 61 GtC/yr the first year (Figure 7a). Nanophytoplankton and diatoms contribute equally to this gain in productivity. However, the relative increase in diatoms is larger, growing from about 20% to 31% of the total primary production. With greater primary productivity, export production increases from 8 GtC/yr to 11.5 GtC/yr. After this sharp initial increase, both primary and export production gradually decrease to reach 50.7 GtC/yr and 9.8 GtC/yr at the end of the simulation. These slow declines result from more efficient consumption and export of the macronutrients in the HNLC regions that reduces their lateral transport to the oligotrophic areas. Thus massive iron fertilization stimulates productivity and export in the HNLC regions at the expense of increasing the severity and the spatial extent of the oligotrophic regions (Figure 8b).

[32] Such a reduction is not surprising as it has been shown previously [*Sarmiento and Orr*, 1991; *Aumont et al.*, 2003]. Two pathways should be at play in the case of iron fertilization. First, the lateral transfer at the surface by the Ekman drift is diminished due to the reduction of the nutrient concentrations in the former HNLC regions. Thus primary productivity is reduced primarily on the borders of the oligotrophic regions [*Williams and Follows*, 1998]. This pathway is rapid, on the order of 1 year. The second pathway operates over much longer timescales but also over the global ocean [*Rodgers et al.*, 2003]. Nitrate concentrations are strongly decreased in the Sub-Antarctic Mode Waters (SAMW). As these waters are the main source of nutrients for the low latitudes, this nutrient depletion should result in an overall and slow reduction of the primary productivity in the low latitudes [*Sarmiento et al.*, 2004].

[33] The addition of iron significantly stimulates the export of organic matter to the subsurface. The ocean becomes thus a larger sink of atmospheric $CO_2$ (Figure 7b). After 100 years, atmospheric $pCO_2$ is reduced by 33 μatm relative to the control simulation (Figure 7c). This corresponds to an additional carbon sequestration of 70 GtC by the ocean which is substantially less than the extra 226 GtC that is exported below 100 m due to stimulated biological activity. This disparity results in part because much of the exported carbon is returned to the upper few hundred meters of the ocean where it is quickly reexposed to the atmosphere. About 90% of the additional uptake occurs in the Southern Ocean confirming the predominant role of this region [*Sarmiento and Orr*, 1991]. Consequently, a negligible impact on atmospheric $pCO_2$ should be expected from an, even massive and permanent, iron fertilization in the tropics or in the northern mid and high latitudes, including the equatorial Pacific.

## 5. Discussion

### 5.1. Atmospheric $CO_2$ Drawdown

[34] The 33-μatm drawdown in atmospheric $CO_2$ predicted by our model is significantly smaller than values

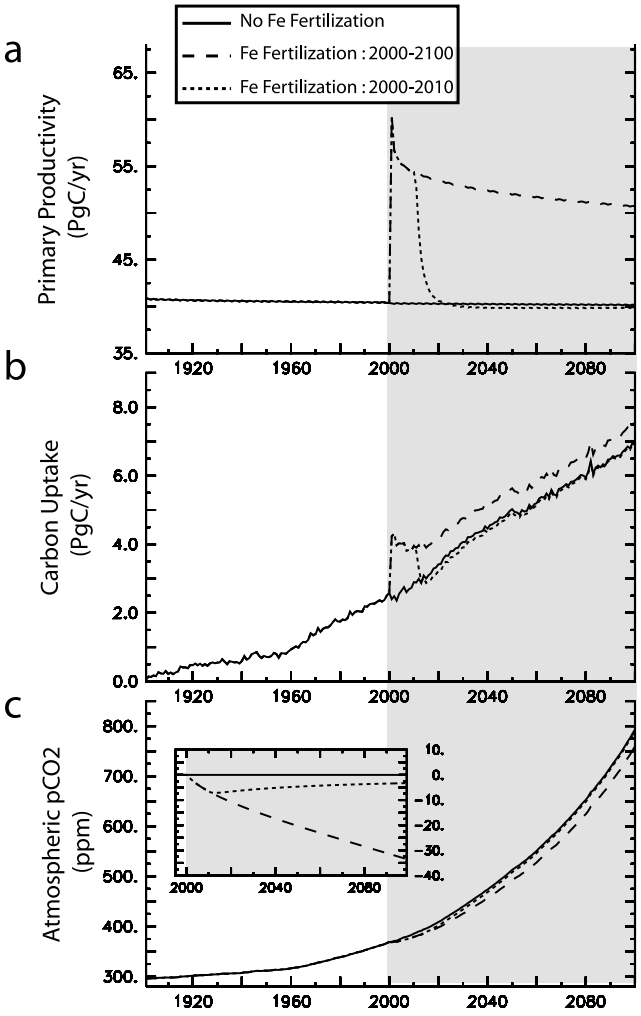



**Figure 7.** Evolution of (a) global primary productivity in PgC $yr^{-1}$, (b) ocean carbon fluxes (positive to the ocean) in PgC $yr^{-1}$, and (c) atmospheric $pCO_2$ in ppmv. The black line represents the experiment in which no iron is added. The long-dashed line represents the standard fertilization experiment. The short-dashed line represents the fertilization experiment in which iron infusion is stopped after 2010 (see text).

reported in previous modeling studies [*Peng and Broecker*, 1991; *Joos et al.*, 1991; *Sarmiento and Orr*, 1991; *Kurz and Maier-Reimer*, 1993] using much simpler biogeochemical models. These models were simulating reductions larger than 50 μatm for experiments including anthropogenic fossil fuel emissions (Table 1). The only exception to these elevated values is given by *Zeebe and Archer* [2005]. Using results from SOFeX and several ocean models, they estimated that iron fertilization would lead to a feasible reduction in atmospheric $CO_2$ of less than 15 ppmv. However, their study is not directly comparable to the other studies (including ours). On the basis of a feasibility assessment regarding the currently available technology, they fertilized the ocean only 15 times a year south of 55°S. In the other studies mentioned here, iron enrichment is performed all year round (only the six summer months of *Kurz and Maier-Reimer* [1993], which were also producing the lowest estimate, i.e., 50 ppmv) over the whole Southern Ocean or over the global ocean. Thus, leaving aside this work by *Zeebe and Archer* [2005], why such a small response in our model when compared to similar studies?

[35] In these previous studies, iron fertilization was simulated by assuming a complete utilization of the surface macronutrients (phosphate or nitrate) all year round (only the six summer months of *Kurz and Maier-Reimer* [1993]). Our model suggests that this assumption is by far too extreme (Figure 8a), especially in the Southern Ocean which is responsible for most of the atmospheric carbon sequestration. Despite a large reduction due to the enhanced biological activity, surface nitrate concentrations always remain at significant levels south of about 50°S. In fact, nitrate and phosphate are never exhausted in this region, even during the most favorable growing season.

[36] The persistence of elevated nitrate concentrations results from the interplay of other limiting factors than iron. First, the stimulation of the biological activity is restricted in this region to the summer season which lasts for only 3 to 6 months (Figure 6). Nutrients can then build up at the surface during wintertime without being consumed very differently than in the unperturbed case. As a result, maximum nitrate concentrations are not significantly altered in the Southern Ocean when iron is artificially supplied. Second, during the favorable season, other limiting factors come into play: Silicon limitation north of the Polar Front, light limitation south of it (Figure 9). These limiting factors often prevent a complete consumption of the macronutrients (Figure 8a), either by slowing down the phytoplankton growth (light limitation) or by stopping the diatoms bloom (silicate limitation). The export production is increased for only several months and to significantly lower values than what a complete removal of surface macronutrients would require. For instance, the perturbation new production averaged 12–14 GtC/yr for *Sarmiento and Orr* [1991] to be compared to the mean 2.5 GtC/yr in our experiment.

[37] Our results support the hypothesis that other limiting factors play a critical role in limiting the efficiency of iron fertilization to sequester atmospheric carbon [*Popova et al.*, 2000]. To more quantitatively estimate this role, we have performed an additional simulation in which nitrate remains as the only control of phytoplankton growth. As expected from our previous analysis, export production is strongly increased to about 20 GtC/yr on average over the 100 years of the simulation, that is, about 12 GtC/yr higher than in the control experiment. Nitrate are almost exhausted everywhere, except in the Ross and the Weddell Seas where the physical model produces very strong and deep winter mixing (not shown). In this extreme case, atmospheric $CO_2$ drawdown reaches 87 ppmv. These values, both for export production and for atmospheric $CO_2$, are very similar to the findings of previous modeling studies (see Table 1).

### 5.2. Efficiency of Iron Fertilization

[38] Our model predicts that about 33% of the additional export produced by the fertilization comes out of the

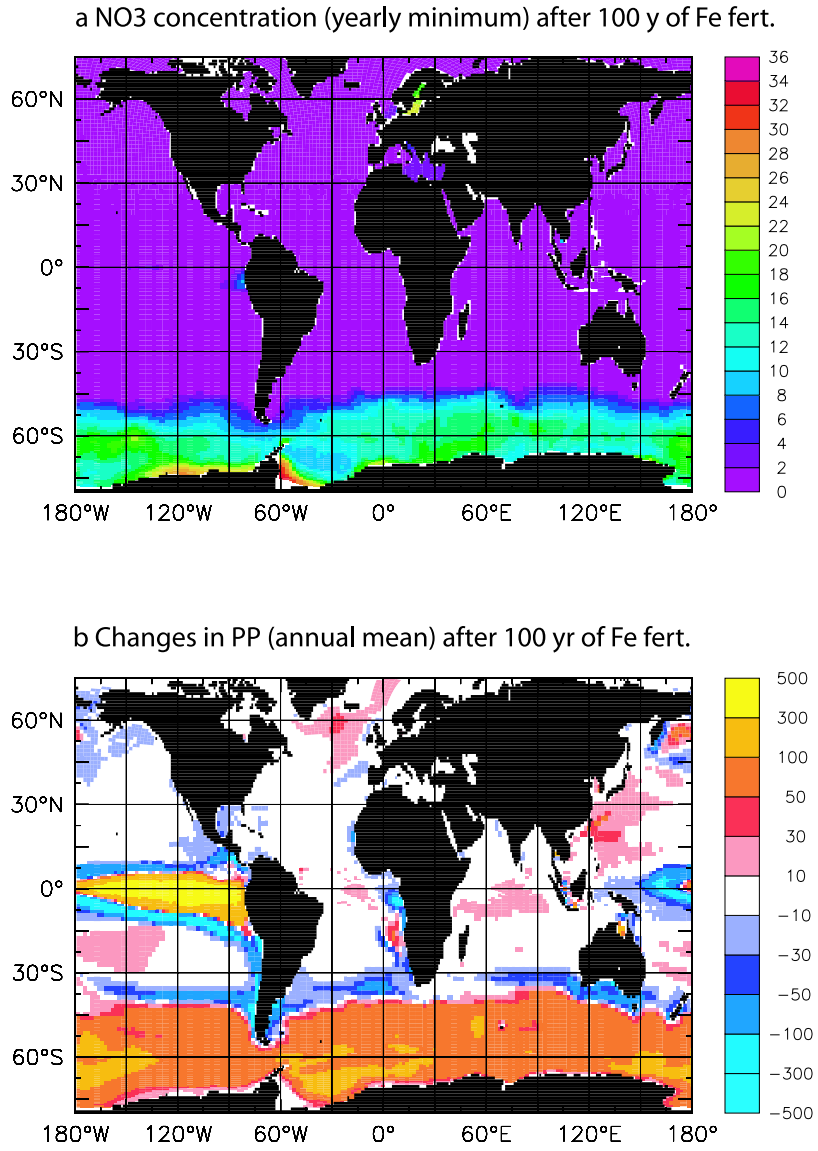



**Figure 8.** (a) Yearly minimum concentrations of nitrate (in mmol/m$^3$) at the surface for the fertilization experiment. (b) Changes in vertically integrated primary productivity (in gC/m$^2$/yr) in the fertilization experiment relative to the control simulation.

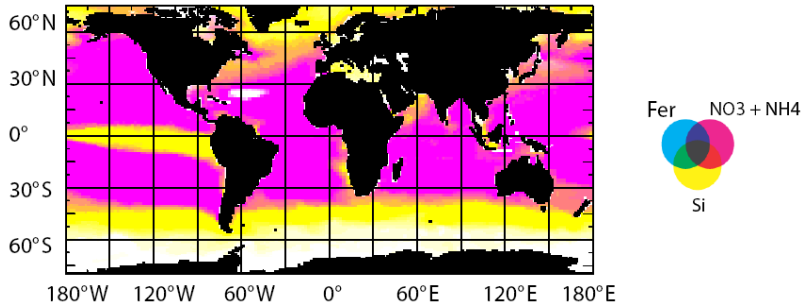



**Figure 9.** Colimitation of diatoms growth for the control experiment in year 2100. Blue, yellow, and pink areas denote, respectively, maximum limitation by iron, silicic acid, and nitrogen (nitrate + ammonium). Light limitation is also represented by a white shading over previous colors.

atmosphere over the 100 years of the experiment. The rest is compensated by increased vertical supply of carbon resulting from the progressive reexposition of the sequestered carbon to the surface. Furthermore, the efficiency is not constant over time. It peaks at about 60% the first year and then decreases to 25% at the end of the simulation as more and more sequestered carbon is brought back to the surface. When iron enrichment is stopped, the efficiency drops rapidly to very low levels, around 6% in year 2100 (Figure 7). Three thoughts can be drawn from these results. (1) Iron fertilization should be performed continuously; otherwise its benefits are lost quickly in agreement with what was found in previous studies [*Sarmiento and Orr*, 1991; *Gnanadesikan et al.*, 2003]. (2) Maintaining the efficiency close to its maximum level would require continuous increase in the export production, which is of course impossible. (3) The amount of sequestered carbon cannot be directly and easily estimated from export flux measurements [*Gnanadesikan et al.*, 2003].

[39] Our efficiency, 33% on average, is significantly higher than what was found in previous studies: 10–25% for *Zeebe and Archer* [2005] and 2–11.5% for *Gnanadesikan et al.* [2003]. Understanding this difference is quite challenging, as the experimental designs differ in many aspects. Nevertheless, the time evolution of our sequestration efficiency is more similar to the ADD-BOTTOM-type experiments of *Gnanadesikan et al.* [2003] in which macronutrients are continuously added to maintain the export production to its prefertilization values and the additional fixed carbon is exported to the bottom of the ocean. This suggests that our higher efficiency can be primarily explained by differences in the biological models.

[40] *Gnanadesikan et al.* [2003] as well as *Zeebe and Archer* [2005] used the nutrient-restoring formulation according to the OCMIP protocols [*Orr*, 1999]. After the iron addition, simulated by imposing surface phosphate concentration to zero, export production drops at the fertilization site but also downstream of it until surface phosphate concentration rises back above its climatological value. This drop induces a loss of carbon to the atmosphere (the ''rebound'' period of *Gnanadesikan et al.* [2003]). In our model, primary and export productions only decrease when nutrients become limiting, i.e., when they fall to very small values. As shown in section 4.2, this reduction is localized in the low latitudes and is generated by reduced lateral advective supply of macronutrients. Thus this ''rebound'' period does indeed exist but requires much longer timescales (years to decades) to fully develop. Around the fertilization sites, biological activity remains high, which is equivalent to adding nutrients in the nutrient-restoring-type models (ADD case of *Gnanadesikan et al.* [2003]). A second explanation for our high efficiency relies on the depth at which organic matter is exported. In our model, fertilization increases mostly the export by the big particles whose average remineralization length scale is about 2000 m. This value is substantially larger than the mean 700 m prescribed by the OCMIP protocols. The consequence is a greater efficiency of the fertilization [*Gnanadesikan et al.*, 2003]. Nevertheless, other processes may act as well, like, for instance, different vertical diffusivity coefficients [*Gnanadesikan et al.*, 2003].

### 5.3. Nonlocal Effects

[41] Using a global ocean model, *Gnanadesikan et al.* [2003] did quite a complete study of iron fertilization analyzing the sensitivity of the response to many different parameters both on the dynamics and on the biogeochemistry. However, because of their very simple biological scheme, they left unanswered some critical questions mostly related to the primary productivity and the iron cycle. Here, since we use a more complex biogeochemical model, we are able to answer some of their questions.

[42] 1. What are the nonlocal effects of fertilization? Previous studies have suggested that iron fertilization may alter the current patterns of primary productivity, even far away from the enrichment sites [*Sarmiento and Orr*, 1991; *Gnanadesikan et al.*, 2003]. However, because they were using the nutrient-restoring approach, export production was predicted to drop to zero after the stop of the iron supply. Of course, as shown by our model, this result is unrealistic. Primary productivity is not decreased in the core of the HNLC regions, neither during the fertilization nor after it. In the equatorial Pacific and north of the Polar Front, there is generally a significant decrease in biological activity relative to the initial peak induced by the fertilization due to light and/or silicon limitations, but this activity always remains higher than in the unperturbed case (Figure 8b). On the other hand, primary productivity is reduced far away from the infusion sites. This reduction spans the whole low latitudes (except the equatorial Pacific), resulting in a larger extent and greater severity of the oligotrophic gyres (see section 4.2). More interestingly, after the stop of the artificial iron supply, the ocean does not return back to its preperturbed state (Figure 7). Together with carbon, nutrients have been routed from the surface to the deep ocean. Consequently, when iron infusion is ceased, primary productivity drops below its prefertilization level for the rest of the experiment. This suggests that iron fertilization may perturb the ocean biological activity, even long after its stop.

[43] 2. How does fertilization affect the location of remineralization? One of the prominent results of the in situ fertilization experiments is that large cells, generally diatoms, contribute to a large extent to the observed increase in the phytoplankton biomass [*de Baar et al.*, 2005]. As a consequence, iron fertilization is expected to lead to a more efficient burial of the exported carbon to the deep ocean [e.g., *Lefèvre and Watson*, 1999]. Our model supports this hypothesis: The larger contribution from the large particles increases the mean sinking speed from 19 m $d^{-1}$ in the unperturbed case to 28 m $d^{-1}$ in the perturbed case at 200 m, and from 54 m $d^{-1}$ to 71 m $d^{-1}$ at 1000 m, respectively. However, change in the size spectrum is only one potential factor among others that may impact on the remineralization length scales. For instance, the composition of the particles, especially in ballast minerals (carbonate, silicate), is critical as demonstrated by *Armstrong et al.* [2002]. Decrease in the silicification of the diatoms as generally observed when iron is no longer limiting [*Takeda*, 1998; *Leynaert et al.*, 2004] may partly offset the increase in the sinking speeds resulting

from the particles larger sizes. Another aspect is the lability of the organic matter. Fresher materials are solubilized faster and thus are shallower in the water column [e.g., *Murnane et al.*, 1996]. Unfortunately, our model is too idealized to explore these processes.

[44] 3. What is the fate of fertilizing agents (like iron) away from the surface layer? The experimental design we adopted in this study to simulate iron enrichment requires an annual Fe input of about $100 \times 10^9$ mol Fe $yr^{-1}$. This value is roughly 20 times the amount of iron that is supplied to the ocean by dust deposition [*Moore et al.*, 2004; *Parekh et al.*, 2004]. Despite this enormous additional input, the ocean iron content is increased by only about 30% after 100 years of continuous fertilization and does not evolve much after that time. In fact, most of the added iron is lost to the sediments by intense scavenging onto particles. Furthermore, when iron fertilization is stopped, this supplementary iron is lost rapidly from the ocean. After 10 years, the iron global content is only about 15% higher than in the nonperturbed case. After 90 years, the artificially added iron has been almost entirely washed out of the ocean, resulting in virtually identical ocean Fe content in both cases. At the surface, the Fe lifetime is even shorter because of the larger particles numbers which create in an intense loss by coagulation and adsorption and because of the biological activity [*Bowie et al.*, 2001; *Croot et al.*, 2004]. In most of the HNLC regions, the stimulation of primary productivity vanishes completely less than 10 years after the stop of the iron infusion. On the contrary, the decrease in primary productivity induced in the low latitudes persists over much longer timescales (see above).

## 6. Conclusions

[45] One (not necessarily desired) outcome of the success of iron fertilization experiments and of previous modeling studies has been to lend credibility to the idea of massively fertilizing the ocean to mitigate increasing atmospheric $CO_2$ [*Chisholm et al.*, 2001; *Buesseler and Boyd*, 2003]. In the light of this study, several thoughts can be drawn. First, iron limitation in the HNLC regions, especially in the Southern Ocean, is not the whole story. Light and silicate limitations play a critical role and generally prevent from a complete utilization of the available macronutrients. These limitations mainly explain the moderate efficiency of iron fertilization in our model in sequestering atmospheric carbon, especially relative to previous modeling studies. Second, fertilizing the ocean outside the Southern Ocean results in a negligible carbon sequestration as only 10% of the 33 μatm is trapped north of 40°S. Third, iron fertilization should be done continuously, as when stopped, a large part of the sequestered carbon is reexposed to the atmosphere quite rapidly.

[46] Finally, the marine ecosystems can be modified even far away from the injection sites, potentially resulting in changes in the distribution and abundance of the marine resources. More problematic, the model suggests that these changes could be lastingly created, as after the stop of the iron infusion, global primary productivity drops rapidly and remains below the unperturbed scenario for the rest of the experiment. Together with other potential side effects that have been identified so far [*Sarmiento and Orr*, 1991; *Gnanadesikan et al.*, 2003; *Jin and Gruber*, 2003], iron fertilization should be warily considered, as it may not be environmentally benign during but also long after its achievement. However, the tool used in this study is a model and even if PISCES is far more complex than the models that were previously used to address artificial iron fertilization, it is still a simplified (and simplistic) representation of reality. Thus large uncertainties remain concerning the efficiency of iron fertilization that should be further explored using more observations and/or other models.

[47] **Acknowledgments.** We thank C. Le Quéré, K. Rodgers, J. C. Orr, P. Monfray, and P. Ciais who helped a lot improving this manuscript. This work was supported by the French PROOF program OCEVAR.

## References

Armstrong, R. A., C. Lee, J. I. Hedges, S. Honjo, and S. G. Wakeham (2002), A new, mechanistic model for organic carbon fluxes in the ocean based on the quantitative association of POC with ballast minerals, *Deep Sea Res., Part II*, *49*, 219–236.

Aumont, O., S. Belviso, and P. Monfray (2002), Dimethylsulfoniopropionate (DMSP) and dimethylsulfide (DMS) sea surface distributions simulated from a global three-dimensional ocean carbon cycle model, *J. Geophys. Res.*, *107*(C4), 3029, doi:10.1029/1999JC000111.

Aumont, O., E. Maier-Reimer, S. Blain, and P. Monfray (2003), An ecosystem model of the global ocean including Fe, Si, P co-limitation, *Global Biogeochem. Cycles*, *17*(2), 1060, doi:10.1029/2001GB001745.

Beckmann, A., and R. Döscher (1997), A method for improved representation of dense water spreading over topography in geopotential-coordinate models, *J. Phys. Oceanogr.*, *27*, 581–591.

Bidigare, R. R., et al. (1999), Iron-stimulated changes in $^{13}C$ fractionation and export by equatorial Pacific phytoplankton: Toward a paleogrowth rate proxy, *Paleoceanography*, *14*, 589–595.

Blanke, B., and P. Delecluse (1993), Low frequency variability of the tropical Atlantic Ocean simulated by a general circulation model with mixed layer physics, *J. Phys. Oceanogr.*, *23*, 1363–1388.

Bowie, A., M. Maldonado, R. Frew, P. Croot, E. Achterberg, R. Mantoura, P. Worsfold, C. Law, and P. Boyd (2001), The fate of added iron during a mesoscale fertilisation experiment in the Southern Ocean, *Deep Sea Res., Part II*, *48*, 2703–2743.

Boyd, P. W. (2004), Ironing out algal issues in the Southern Ocean, *Science*, *304*, 396–397.

Boyd, P. W., et al. (2000), A mesoscale phytoplankton bloom in the polar Southern Ocean stimulated by iron fertilization, *Nature*, *407*, 695–702.

Boyd, P. W., et al. (2004), The decline and fate of an iron-induced subarctic phytoplankton bloom, *Nature*, *428*, 549–553.

Bozec, Y., D. C. E. Bakker, C. Hartmann, H. Thomas, R. G. J. Bellerby, P. D. Nightingale, U. Riebesell, A. J. Watson, and H. J. W. de Baar (2005), The $CO_2$ system in a Redfield context during an iron enrichment experiment in the Southern Ocean, *Mar. Chem.*, *95*, 89–105.

Bruland, K. W., E. L. Rue, G. J. Smith, and G. R. DiTullio (2005), Iron, macronutrients and diatom blooms in the Peru upwelling regime: Brown and blue waters of Peru, *Mar. Chem.*, *93*, 81–103.

Buesseler, K. O., and P. W. Boyd (2003), Will ocean fertilization work?, *Science*, *300*, 67–68.

Buesseler, K. O., J. E. Andrews, S. M. Pike, and M. A. Charette (2004), The effects of iron fertilization on carbon sequestration in the Southern Ocean, *Science*, *304*, 414–417.

Cavender-Bares, K. K., E. L. Mann, S. W. Chisholm, M. E. Ondrusek, and R. R. Bidigare (1999), Differential response of equatorial Pacific phytoplankton to iron fertilization, *Limnol. Oceanogr.*, *44*, 237–246.

Chisholm, S. W., P. G. Falkowski, and J. J. Cullen (2001), Dis-crediting ocean fertilization, *Science*, *294*, 309–310.

Coale, K. H., et al. (1996), A massive phytoplankton bloom induced by an ecosystem-scale iron fertilization experiment in the equatorial Pacific Ocean, *Nature*, *383*, 495–501.

Coale, K. H., et al. (2004), Southern Ocean Iron Enrichment Experiment: Carbon cycling in high- and low-Si waters, *Science*, *304*, 408–414.

Conkright, M. E., R. A. Locarnini, H. E. Garcia, T. D. O'Brien, T. P. Boyer, C. Stephens, and J. Antononov (2002), World Ocean Atlas 2001: Objective Analyses, Data Statistics and Figures [CD-ROM], *NOAA Atlas NESDIS 42*, Silver Spring, Md.

Croot, P. L., P. Streu, and A. R. Baker (2004), Short residence time for iron in surface seawater impacted by atmospheric dry deposition from Saharan dust events, *Geophys. Res. Lett.*, *31*, L23S08, doi:10.1029/2004GL020153.

de Baar, H. J. W., and J. T. M. de Jong (2001), Distributions, sources and sinks of iron in seawater, in *The Biogeochemistry of Iron in Seawater*, edited by D. Turner and K. Hunter, pp. 85–121, John Wiley, Hoboken, N. J.

de Baar, H., et al. (2005), Synthesis of iron fertilization experiments: From the Iron Age in the Age of enlightenment, *J. Geophys. Res.*, *110*, C09S16, doi:10.1029/2004JC002601.

Dufresne, J. L., P. Friedlingstein, M. Berthelot, L. Bopp, P. Ciais, L. Fairhead, H. LeTreut, and P. Monfray (2002), Effects of climate change due to $CO_2$ increase on land and ocean carbon uptake, *Geophys. Res. Lett.*, *29*(10), 1405, doi:10.1029/2001GL013777.

Dugdale, R. C., and F. P. Wilkerson (1998), Silicate regulation of new production in the equatorial Pacific upwelling, *Nature*, *391*, 270–273.

Dutkiewicz, S., M. J. Follows, and P. Parekh (2005), Interactions of the iron and phosphorus cycles: A three-dimensional model study, *Global Biogeochem. Cycles*, *19*, GB1021, doi:10.1029/2004GB002342.

Franck, V. M., M. A. Brzezinski, K. H. Coale, and D. M. Nelson (2000), Iron and silicic acid concentrations regulate Si uptake north and south of the Polar Frontal Zone in the Pacific Sector of the Southern Ocean, *Deep Sea Res., Part II*, *47*, 3315–3338.

Gall, M. P., P. W. Boyd, J. Hall, K. A. Safi, and H. Chang (2001), Phytoplankton processes: Part 1. Community structure during the Southern Ocean Iron RElease Experiment (SOIREE), *Deep Sea Res., Part II*, *48*, 2551–2570.

Geider, R. J., H. L. MacIntyre, and T. M. Kana (1998), A dynamic regulatory model of phytoplanktonic acclimation to light, nutrients, and temperature, *Limnol. Oceanogr.*, *43*, 679–694.

Gent, P. R., and J. C. McWilliams (1990), Isopycnal mixing in ocean circulation models, *J. Phys. Oceanogr.*, *20*, 150–155.

Gervais, F., U. Riebesell, and M. Y. Gorbunov (2002), Changes in primary productivity and chlorophyll a in response to iron fertilization in the Southern Polar Frontal Zone, *Limnol. Oceanogr.*, *47*, 1324–1335.

Gnanadesikan, A., R. J. Slater, N. Gruber, and J. L. Sarmiento (2002), Oceanic vertical exchange and new production: A comparison between models and observations, *Deep Sea Res., Part II*, *49*, 363–401.

Gnanadesikan, A., J. L. Sarmiento, and R. D. Slater (2003), Effects of patchy ocean fertilization on atmospheric carbon dioxide and biological production, *Global Biogeochem. Cycles*, *17*(2), 1050, doi:10.1029/2002GB001940.

Gnanadesikan, A., J. P. Dunne, R. M. Key, K. Matsumoto, J. L. Sarmiento, R. D. Slater, and P. S. Swathi (2004), Oceanic ventilation and biogeochemical cycling: Understanding physical mechanisms that produce realistic distributions of tracers and productivity, *Global Biogeochem. Cycles*, *18*, GB4010, doi:10.1029/2003GB002097.

Goose, H. (1997), Modelling the large-scale behaviour of the coupled ocean-sea-ice system, Ph.D. thesis, 231 pp., Univ. Cath. de Louvain, Louvain-La-Neuve, Belgium.

Gregg, W., P. Ginoux, P. Schopf, and N. Casey (2003), Phytoplankton and iron: Validation of global three-dimensional ocean biogeochemical model, *Deep Sea Res., Part II*, *50*, 3143–3169.

Gribbin, J. (1988), Any old iron?, *Nature*, *331*, 570.

Hutchins, D. A., and K. W. Bruland (1998), Iron-limited diatom growth and Si:N uptake ratios in a coastal upwelling regime, *Nature*, *393*, 561–564.

Jickells, T. D., and L. J. Spokes (2001), Atmospheric iron inputs to the oceans, in *The Biogeochemistry of Iron in Seawater*, edited by D. Turner and K. Hunter, pp. 85–121, John Wiley, Hoboken, N. J.

Jin, X., and N. Gruber (2003), offsetting the radiative benefit of ocean iron fertilization by enhancing $N_2O$ emissions, *Geophys. Res. Lett.*, *30*(24), 2249, doi:10.1029/2003GL018458.

Johnson, K. S., F. P. Chavez, and G. E. Friederich (1999), Continental-shelf sediment as a primary source of iron for coastal phytoplankton, *Nature*, *398*, 697–700.

Joos, F., J. L. Sarmiento, and U. Siegenthaler (1991), Estimates of the effect of Southern-Ocean iron fertilization on atmospheric $CO_2$ concentrations, *Nature*, *349*, 772–775.

Kalnay, E. C., et al. (1996), The NCEP/NCAR Reanalysis Project, *Bull. Am. Meteorol. Soc.*, *77*, 437–471.

Kurz, K. D., and E. Maier-Reimer (1993), Iron fertilization of the Austral Ocean: The Hamburg model assessment, *Global Biogeochem. Cycles*, *7*, 229–244.

Lefèvre, N., and A. J. Watson (1999), Modeling the geochemical cycle of iron in the oceans and its impact on atmospheric $CO_2$ concentrations, *Global Biogeochem. Cycles*, *13*, 727–736.

Lengaigne, M., G. Madec, C. Menkes, and G. Alory (2003), Effect of isopycnal diffusion in the tropical Pacific Ocean, *J. Geophys. Res.*, *108*(C11), 3345, doi:10.1029/2002JC001704.

Leynaert, A., E. Bucciarelli, P. Claquin, R. C. Dugdale, V. Martin-Jézéquel, P. Pondaven, and O. Ragueneau (2004), Effect of iron deficiency on diatom cell size and silicic acid uptake kinetics, *Limnol. Oceanogr.*, *49*, 1134–1143.

Ludwig, W., J. L. Probst, and S. Kempe (1996), Predicting the oceanic input of organic carbon by continental erosion, *Global Biogeochem. Cycles*, *10*, 23–41.

Madec, G., P. Delecluse, M. Imbard, and C. Lévy (1998), OPA8.1 Ocean general circulation model reference manual, *Notes du pôle de modél. 11*, 91 pp., Inst. Pierre-Simon Laplace, Paris.

Martin, J. H. (1990), Glacial-interglacial $CO_2$ change: The iron hypothesis, *Paleoceanography*, *5*, 1–13.

Martin, J. H., and S. E. Fitzwater (1988), Iron deficiency limits phytoplankton growth in the northeast Pacific subarctic, *Nature*, *331*, 341–343.

Martin, J. H., R. M. Gordon, and S. E. Fitzwater (1990), Iron in the antarctic waters, *Nature*, *345*, 156–158.

Martin, J. H., et al. (1994), Testing the iron hypothesis in ecosystems in the equatorial Pacific, *Nature*, *371*, 123–129.

Matear, R., and C. S. Wong (1999), Potential to increase the oceanic $CO_2$ uptake by enhancing marine productivity in high nutrient low chlorophyll regions, in *Greenhouse Gas Control Technologies*, edited by B. Eliasson, P. Reimer, and A. Wokaun, pp. 281–286, Elsevier, New York.

Measures, C., and S. Vink (1999), Seasonal variations in the distribution of Fe and Al in the surface waters of the Arabian Sea, *Deep Sea Res., Part II*, *46*, 11,597–11,622.

Menkes, C., J.-P. Boulanger, A. J. Busalacchi, J. J. Vialard, P. Delecluse, M. J. McPhaden, E. Hackert, and N. Grima (1998), Impact of TAO vs. ERS wind stresses onto simulations of the tropical Pacific Ocean during the 1993–1998 period by the OPA OGCM, in *Climatic Impact of Scale Interactions for the Tropical Ocean-Atmosphere System*, pp. 46–48, EuroClivar, Paris.

Monod, J. (1942), *Recherches sur la Croissance des Cultures Bactériennes*, Hermann, Paris.

Moore, J. K., S. C. Doney, J. A. Kleypas, D. M. Glover, and I. Y. Fung (2002), An intermediate complexity marine ecosystem model for the global domain, *Deep Sea Res., Part II*, *49*, 403–462.

Moore, J. K., S. C. Doney, and K. Lindsay (2004), Upper ocean ecosystem dynamics and iron cycling in a global three-dimensional model, *Global Biogeochem. Cycles*, *18*, GB4028, doi:10.1029/2004GB002220.

Murnane, R. J., J. K. Cochran, K. O. Buesseler, and M. P. Bacon (1996), Least-square estimates of thorium, particle and nutrient cycling rate constants from the JGOFS North Atlantic Bloom Experiment, *Deep Sea Res., Part I*, *43*, 239–258.

Nakisenovic, N., et al. (2000), *IPCC Special Report on Emissions Scenarios*, Cambridge Univ. Press, New York.

Nishioka, J., S. Takeda, C. S. Wong, and W. K. Johnson (2001), Size-fractionated iron concentrations in the northeast Pacific Ocean: Distribution of soluble and small colloidal iron, *Mar. Chem.*, *74*, 157–179.

Nodder, S. D., M. A. Charette, A. M. Waite, T. W. Trull, P. W. Boyd, J. Zeldis, and K. O. Buesseler (2001), Particle transformations and export flux during an in situ iron-stimulated algal bloom in the Southern Ocean, *Geophys. Res. Lett.*, *28*, 2409–2412.

Orr, J. C. (1999), On ocean carbon-cycle model comparison, *Tellus, Ser. B*, *51*, 509–510.

Parekh, P., M. J. Follows, and E. A. Boyle (2004), Decoupling of iron and phosphate in the global ocean, *Global Biogeochem. Cycles*, GB2020, doi:10.1029/2004GB002280.

Peng, T. H., and W. S. Broecker (1991), Dynamic limitations on the Antarctic iron fertilization strategy, *Nature*, *349*, 227–229.

Platt, T., S. Sathyendranath, A. M. Edwards, D. S. Broomhead, and O. Ulloa (2003), Nitrate supply and demand in the mixed layer of the ocean, *Mar. Ecol. Prog. Ser.*, *254*, 3–9.

Popova, E. E., V. A. Ryabchenko, and M. J. R. Fasham (2000), Biological pump and vertical mixing in the Southern Ocean: Their impact on atmospheric $CO_2$, *Global Biogeochem. Cycles*, *14*, 477–498.

Rodgers, K. B., B. Blanke, G. Madec, O. Aumont, P. Ciais, and J. C. Dutay (2003), Extratropical sources of Equatorial Pacific upwelling in an OGCM, *Geophys. Res. Lett.*, *30*(2), 1084, doi:10.1029/2002GL016003.

Rossow, W. B., and R. A. Schiffer (1999), Advances in understanding clouds from ISCCP, *Bull. Am. Meteorol. Soc.*, *80*, 2261–2288.

Sarmiento, J. L., and J. C. Orr (1991), Three-dimensional simulations of the impact of Southern Ocean nutrient depletion on atmospheric $CO_2$ and ocean chemistry, *Limnol. Oceanogr.*, *36*, 1928–1950.

Sarmiento, J. L., N. Gruber, M. A. Brzezinski, and J. P. Dunne (2004), High-latitude controls of thermocline nutrients and low-latitude biological productivity, *Nature*, *427*, 56–60.

Sarthou, G., et al. (2003), Atmospheric iron deposition and sea-surface dissolved iron concentrations in the eastern Atlantic Ocean, *Deep Sea Res., Part I*, *50*, 1339–1352.

Sedwick, P. N., G. R. DiTullio, and D. J. Mackey (2000), Iron and manganese in the Ross Sea, Antarctica: Seasonal iron limitation in Antarctic shelf waters, *J. Geophys. Res.*, *105*, 11,321–11,336.

Sunda, W. G., and S. A. Huntsman (1995), Iron uptake and growth limitation in oceanic and coastal phytoplankton, *Mar. Chem.*, *50*, 189–206.

Takahashi, T., W. S. Broecker, and S. Langer (1985), Redfield ratio based on chemical data from isopycnal surfaces, *J. Geophys. Res.*, *90*, 6907–6924.

Takeda, S. (1998), Influence of iron availability on nutrient consumption ratio of diatoms in oceanic waters, *Nature*, *393*, 774–777.

Tegen, I., and I. Fung (1995), Contribution to the atmospheric mineral aerosol load from land surface modification, *J. Geophys. Res.*, *100*, 18,707–18,726.

Timmermann, R., H. Goose, G. Madec, T. Fichefet, C. Ethé, and V. Dulière (2003), On representation of high latitude processes in the ORCALIM global coupled sea ice-ocean model, *Ocean Modell.*, *8*, 175–201.

Trenberth, K. E., J. G. Olson, and W. G. Large (1989), A global ocean wind stress climatology based on the ECMWF analyses, *NCAR/TN-338+STR*, Natl. Cent. for Atmos. Res., Boulder, Colo.

Tsuda, A., et al. (2003), A mesoscale iron enrichment in the western subarctic Pacific induces a large centric diatom bloom, *Science*, *300*, 958–961.

Vink, S., and C. Measures (2001), The role of dust deposition in determining surface water distributions of Al and Fe in the south west Atlantic, *Deep Sea Res., Part II*, *48*, 2787–2809.

Williams, R. G., and M. J. Follows (1998), The Ekman transfer of nutrients and maintenance of new production over the North Atlantic, *Deep Sea Res., Part I*, *45*, 461–489.

Xin, P., and P. A. Arkin (1997), Global precipitation: A 17-year monthly analysis based on gauge observations, satellite estimations, and numerical model inputs, *Bull. Am. Meteorol. Soc.*, *78*, 2539–2558.

Zeebe, R. E., and D. Archer (2005), Feasibility of ocean fertilization and its impact on future atmospheric $CO_2$ levels, *Geophys. Res. Lett.*, *32*, L09703, doi:10.1029/2005GL022449.

O. Aumont, Laboratoire d'Océanographie et de Climatologie: Expérimentation et Approches Numériques, IPSL, Centre IRD de Bretagne, BP70, F-29280 Plouzané, France. (olivier.aumont@ird.fr)

L. Bopp, Laboratoire des Sciences du Climat et de l'Environnement, CE Saclay, L'Orme des Merisiers, F-91191 Gif-sur-Yvette Cedex, France. (bopp@lsce.saclay.cea.fr)